JMEPEG (2016) 25:719–725
DOI: 10.1007/s11665-016-1941-7

1059-9495/$19.00

Improved Corrosion Resistance of As-Extruded GZ51K Biomagnesium Alloy with High Mechanical Properties by Aging Treatment

Xiaobo Zhang, Qian Wang, Zhixin Ba, Zhangzhong Wang, and Yajun Xue

(Submitted August 19, 2015; in revised form January 20, 2016; published online February 9, 2016)

Effects of aging treatment on microstructure, mechanical properties, and corrosion behavior of the as-extruded Mg-5Gd-1Zn-0.6Zr (GZ51K, wt.%) alloy were investigated. Microstructure was observed by optical microscopy and scanning electron microscopy, mechanical properties were tested on a tensile test machine and a microhardness tester, and corrosion behavior was evaluated by mass loss and polarization tests. It is found that most of equiaxed α-Mg grains have long-period stacking ordered (LPSO) structure, and some of them have no LPSO structure. Long-elongated grains are formed in the as-extruded alloy due to partial recrystallization and disappear after being aged at 200 and 220 °C. The as-extruded alloy exhibits both high-yield strength and high ductility. The mechanical properties of the alloy are not apparently enhanced, but the corrosion resistance is significantly improved after aging treatment. Moreover, the alloy with LPSO structure presents uniform corrosion mode in simulated body fluid. The GZ51K alloy with high mechanical properties and uniform corrosion behavior is worthy to be further investigated for biomedical applications.

Keywords aging treatment, biomaterial, corrosion, LPSO, magnesium alloy, mechanical property

1. Introduction

Compared with traditional metallic biomaterials, biodegradable magnesium alloys are the rising stars as the next generation biomedical materials, especially for orthopedic and cardiovascular stent applications, thanks to their desirable biodegradability, biocompatibility, and other mechanical and physical properties close to human tissues (Ref 1-3). They may afford temporary support during the service and degrade gradually, which can eliminate follow-up surgery to remove the implant after the tissue has sufficiently healed, and reduce the risk of local inflammation after long-term implantation compared to the traditional metallic implants (Ref 4, 5). Therefore, more and more attention has been attracted on the design and development of novel biodegradable magnesium alloys in recent years (Ref 6-10).

A combination of high strength and simultaneously high ductility is desired for magnesium alloys as temporary implants, such as bone plates, screws, and cardiovascular stents (Ref 11-13). The mechanical properties of the implants will be reduced gradually in vivo if the magnesium alloy degrades uniformly. Otherwise, the mechanical integrity may be prematurely lost if it undergoes localized corrosion mode (Ref 14). Consequently, as a biodegradable magnesium alloy, it should not only have high strength and ductility simultaneously, but also exhibit appropriate corrosion resistance and uniform corrosion mechanism (Ref 15).

High strength (tensile yield strength is over 200 MPa) or high ductility (elongation is over 20%) is able to be obtained separately by hot deformation (Ref 13, 16-18), but both of them can be hardly achieved simultaneously. Furthermore, few of the magnesium alloys exhibit uniform corrosion mode (Ref 9, 19). So it is of great significance to develop novel magnesium alloys with high strength, high ductility, excellent corrosion resistance, and uniform corrosion characteristics for biomedical applications. The GZ51K alloy with LPSO structure under as-cast and solution-treated conditions presents good corrosion resistance and uniform corrosion mode, which is a promising biodegradable magnesium alloy according to our previous studies (Ref 9, 20). In this work, aging treatment was conducted on the as-extruded GZ51K alloy, and microstructure, mechanical properties and corrosion behavior were studied.

2. Experimental

The as-extruded GZ51K rods (hot extruded at 320 °C with an extruded speed of 2 mm/s and an extrusion ratio of 9:1, denoted as E) were aged at 180, 200, and 220 °C for 12 h, respectively (denoted as EA180, EA200 and EA220, respectively). Microstructure of the polished and etched samples was observed using an optical microscope (OM) and a scanning electron microscope (SEM) equipped with an energy dispersive spectrometer (EDS). Hardness of the alloys was evaluated by a microhardness tester under a load of 100 g and a dwell time of 10 s, and the results were averaged from 10 points for each group. Tensile properties of the E and EA200 were tested along extrusion direction at room temperature by a tensile test

Xiaobo Zhang, Qian Wang, Zhixin Ba, Zhangzhong Wang, and **Yajun Xue**, School of Materials Science and Engineering, Nanjing Institute of Technology, Nanjing 211167, China; and Jiangsu Key Laboratory of Advanced Structural Materials and Application Technology, Nanjing 211167, China. Contact e-mail: xbxbzhang2003@163.com.

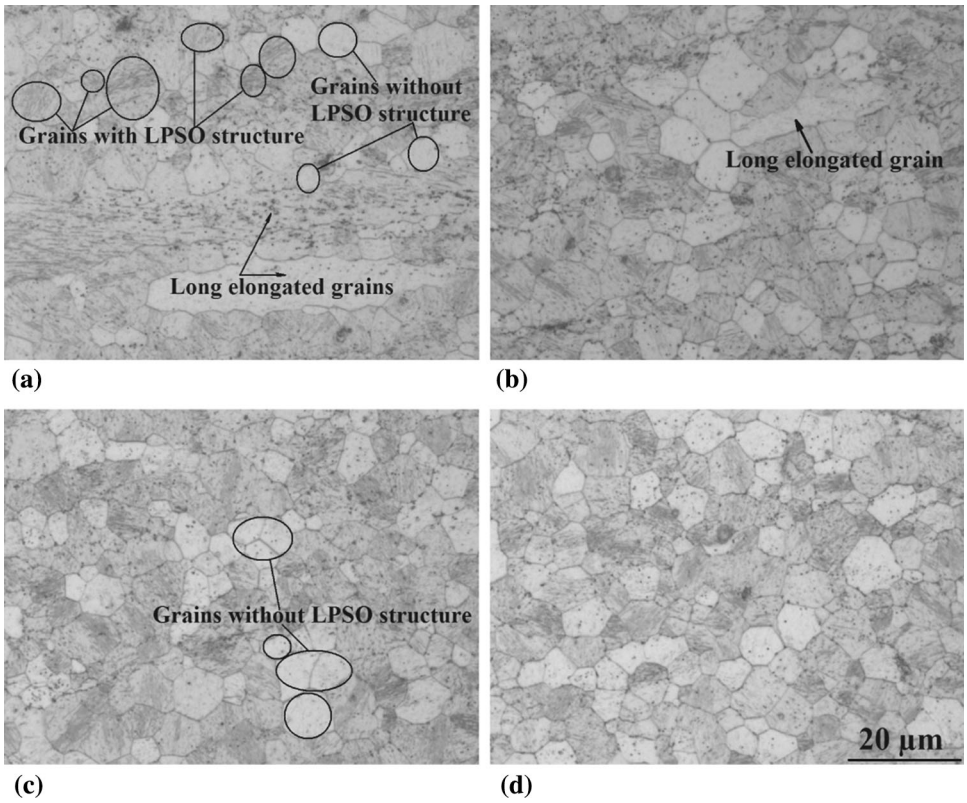

Fig. 1 Optical images of the GZ51K alloys. (a) E, (b) EA180, (c) EA200, (d) EA220

machine with a tensile speed of 1 mm/min, and each sample condition was conducted in triplicate.

Corrosion resistance of the alloy was evaluated by mass loss and polarization tests in this study. The polished disks with a dimension of Ø14 mm × 3.5 mm were immersed in simulated body fluid (SBF) at 37 °C for 120 h. The SBF is composed of NaCl (8.0 g/L), KCl (0.4 g/L), $NaHCO_3$ (0.35 g/L), $MgSO_4 \cdot 7H_2O$ (0.2 g/L), $CaCl_2$ (0.14 g/L), glucose (1 g/L), Na_2HPO_4 (0.06 g/L), and KH_2PO_4 (0.06 g/L). The sample surface area to the SBF volume is approximately 1 cm^2: 60 mL referred to ASTM G31-72. The SBF was replaced every 24 h to keep a stable pH value. After being immersed in SBF for 120 h, the corrosion products and cross sections of the immersed samples were observed by SEM. Corrosion products were removed by 200 g/L chromic acid and 10 g/L silver nitrate solution. Four samples per batch were measured for each condition, and the corrosion rates were determined by mass loss during the immersion test using the following equation (Ref 21):

$$V_{\text{corr}} = \frac{8.76 \times 10^4 \Delta w}{At\rho}, \quad \text{(Eq 1)}$$

where V_{corr} (mm/year) is the corrosion rate of the alloy, Δw (g) is the weight loss, A (cm^2) is the exposed surface area of the specimen, t (h) is the immersion time, and ρ (g/cm^3) is the density of the alloy. The polarization curves of three specimens per batch were evaluated in SBF at 37 °C by a standard three-electrode glass cell with a scan rate of 1 mV/s. The electrochemical parameters were acquired by Tafel extrapolation, and the corrosion rates were approximately converted to mm/year using the following standard equation (Ref 21):

$$P_i = 22.85 i_{\text{corr}}, \quad \text{(Eq 2)}$$

where P_i (mm/year) is the corrosion rate, and i_{corr} (mA/cm^2) is the corrosion current density.

3. Results and Discussion

3.1 Microstructure

Figure 1 shows the optical images of the GZ51K alloys. The microstructure of the as-extruded alloy is composed of equiaxed α-Mg grains with LPSO structure, equiaxed α-Mg grains without LPSO structure, long-elongated grains, and tiny precipitations. The equiaxed grains were formed during hot extrusion due to recrystallization, while the long-elongated grains were elongated from the former large grains which did not undergo recrystallization because of the insufficient stored plastic energy. The LPSO structure distributes throughout the whole grains in the E and EA alloys, while it distributes near the grain boundary within the α-Mg grains in the as-cast and solution-treated conditions (Ref 9, 20) and contains more Gd, Zn, and Zr element than the α-Mg grains without LPSO structure. It is visible that most of the grains have the LPSO structure, and the LPSO structure has a specific orientation in the same grain. The long-elongated grains were still observed after being aged at 180 °C but were not observed after being aged at 200 and 220 °C, indicating that they disappeared owing to static recrystallization. Apart from this, no evident difference could be told between the as-extruded microstructure and the aged ones. Based on the microstructure of the as-extruded and

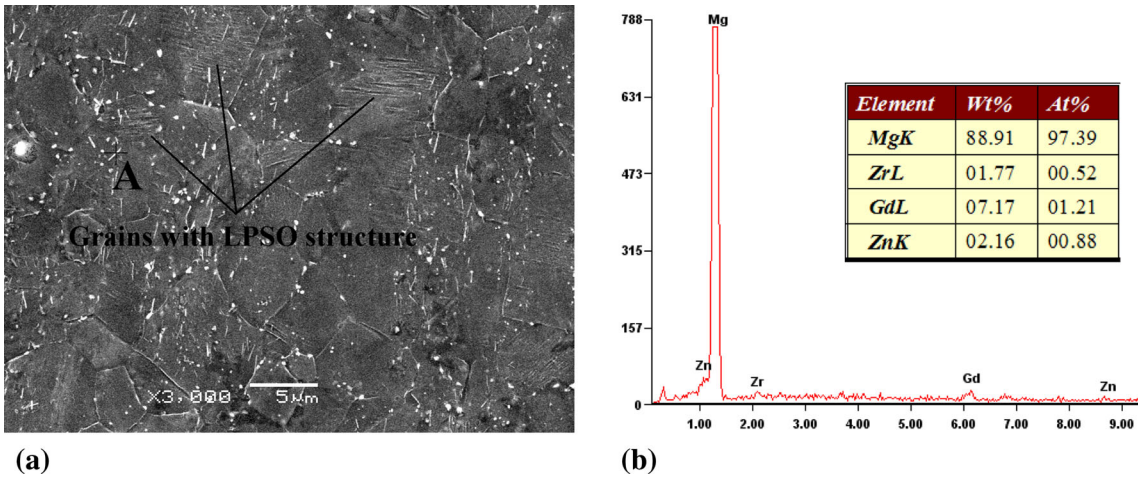

Element	Wt%	At%
MgK	88.91	97.39
ZrL	01.77	00.52
GdL	07.17	01.21
ZnK	02.16	00.88

Fig. 2 SEM micrograph of the EA200 (a) and EDS result of precipitation (b)

aged alloy, it is speculated that the most of the equiaxed grains in the as-extruded alloy are attributed to dynamic recrystallization, but some of them are caused by static recrystallization because of residual energy after extrusion.

The SEM micrograph of the EA200 is shown in Fig. 2(a). The equiaxed grains with LPSO, the equiaxed grains without LPSO, and tiny bright precipitations both in the grain interiors and grain boundaries are observed. Some of the bright precipitations are needle-like, and the others are spherical. They are probably the same phase but with different orientations. The EDS result of the needle-like precipitation presented in Fig. 2(b) reveals that the precipitation contains more Zr, Gd, and Zn than the matrix.

3.2 Mechanical Properties

Microhardness of the alloy is plotted in Fig. 3(a). It increases slightly and then declines with increasing aging temperature, and the highest microhardness is acquired while being aged at 200 °C, which shows only 8% improvement compared to the E. So the tensile test was conducted on the E and EA200, and the results are presented in Fig. 3(b). The yield strength, ultimate tensile strength, and elongation of E and EA200 are 213, 265 MPa, 30.7%, 212, 285 MPa, and 25.0%, respectively. Compared with the as-extruded alloy, the EA200 has similar yield strength, a little higher ultimate tensile strength, and lower elongation.

It has been reported that the as-extruded Mg-Gd-Zn-Zr (Ref 22-25) and Mg-Zn-Y (Ref 26, 27) alloys with LPSO structure exhibit excellent tensile yield strength and also good ductility with appropriate deformed parameters. The strengthening mechanism of the as-extruded magnesium alloy could be attributed to the suppression of dislocation movements and the formation of kink band caused by LPSO structure, as well as grain refinement (Ref 22, 26, 27). The microcrack nucleation and propagation reduced by the kink band, lack of deformation twins (Ref 28), and grain refinement are responsible for good ductility of the magnesium alloys. Consequently, a combination of good yield strength (213 MPa) and elongation (30.7%) of the GZ51K alloy is due to the existence of LPSO structure and refined microstructure.

The higher ultimate tensile strength of the EA200 could be attributed to significant work hardening during tensile test.

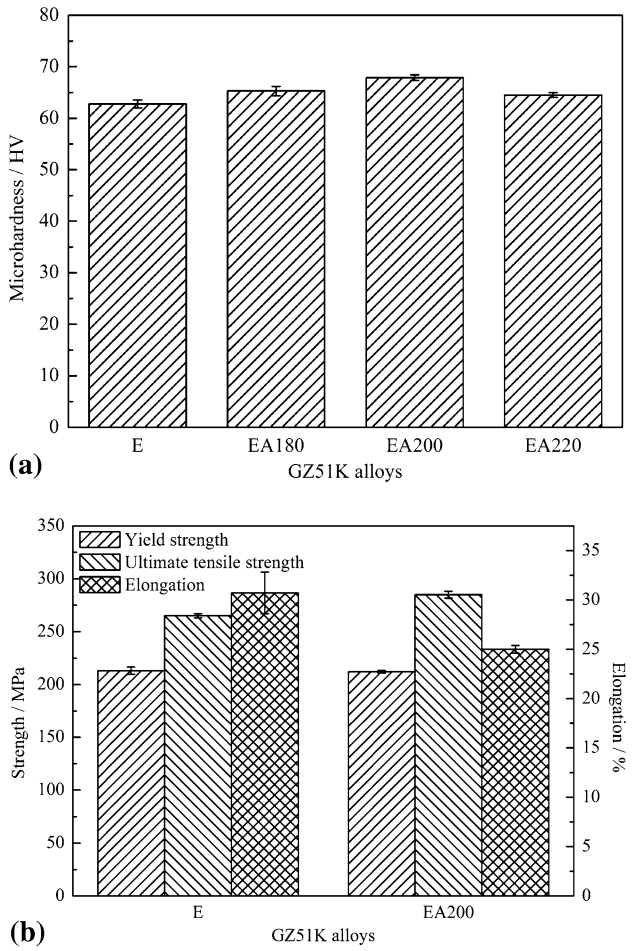

Fig. 3 Mechanical properties of the GZ51K alloys. (a) Microhardness and (b) Tensile properties

However, the yield strength presents no visible improvement. After being aged at 200 °C, the precipitation may lead to improvement of the yield strength due to precipitation strengthening, nevertheless, the static recrystallization for the long-elongated grains could relieve work hardening caused by the deformed microstructure, and the dislocation density may

also be reduced by aging treatment. Therefore, the yield strength of the EA200 is close to that of the E.

3.3 Corrosion Behavior

Corrosion rates of the alloys obtained by four specimens for each group after immersion in SBF for 120 h are presented in Fig. 4. The corrosion rates of the E, EA180, EA200, and EA220 are 0.92, 0.62, 0.50, and 0.53 mm/year, respectively, indicating a significant improvement of corrosion resistance after aging treatment.

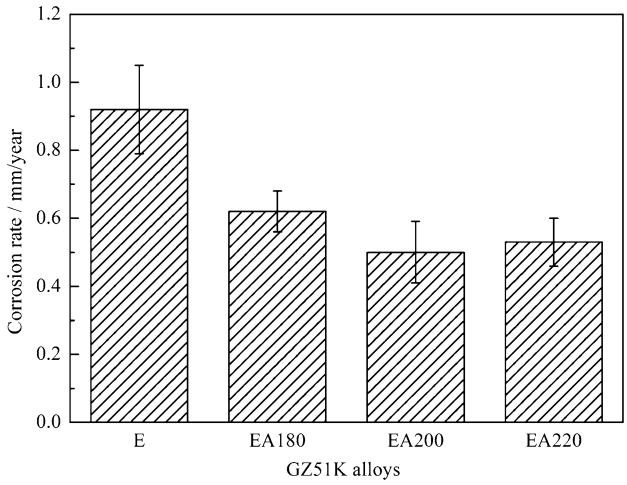

Fig. 4 Corrosion rates of the GZ51K alloys

Figure 5 shows the corrosion morphology of the EA200 and EDS results. The corroded layer was separated by microcracks formed during drying the immersed specimens because of dehydration. Lots of worm-like strips were formed on the surface of the corroded layer. EDS results shown in Fig. 5(b) and (c) indicate that the worm-like strip contains more Mg, Gd, Zn, and less O than the corroded layer. The worm-like strips may correspond to the needle-like precipitation that owns more positive corrosion potential and better corrosion resistance than α-Mg matrix. Therefore, the matrix around them corroded completely, but they still retained the former shape. Ca and P from the SBF precipitated on them during immersion, and resulted in coarser and less straight outline compared to the needle-like precipitations, as shown in Fig. 2(a).

Cross-section morphologies of the immersed specimens in SBF for 120 h are shown in Fig. 6. The thickness of the corroded layer of the EA200 is thinner than that of the E, suggesting that the EA200 presents better corrosion resistance. Both corroded layers are relatively smooth, indicating uniform corrosion mode of the alloys. In addition, the microcracks can be observed on the corroded layer of the EA200, which is consistent with Fig. 5(a). The corroded surfaces (Fig. 7) of the E and EA200 after immersion in SBF for 120 h and removing corrosion products are smooth, which are also predominant evidences that the alloys exhibit uniform corrosion mode.

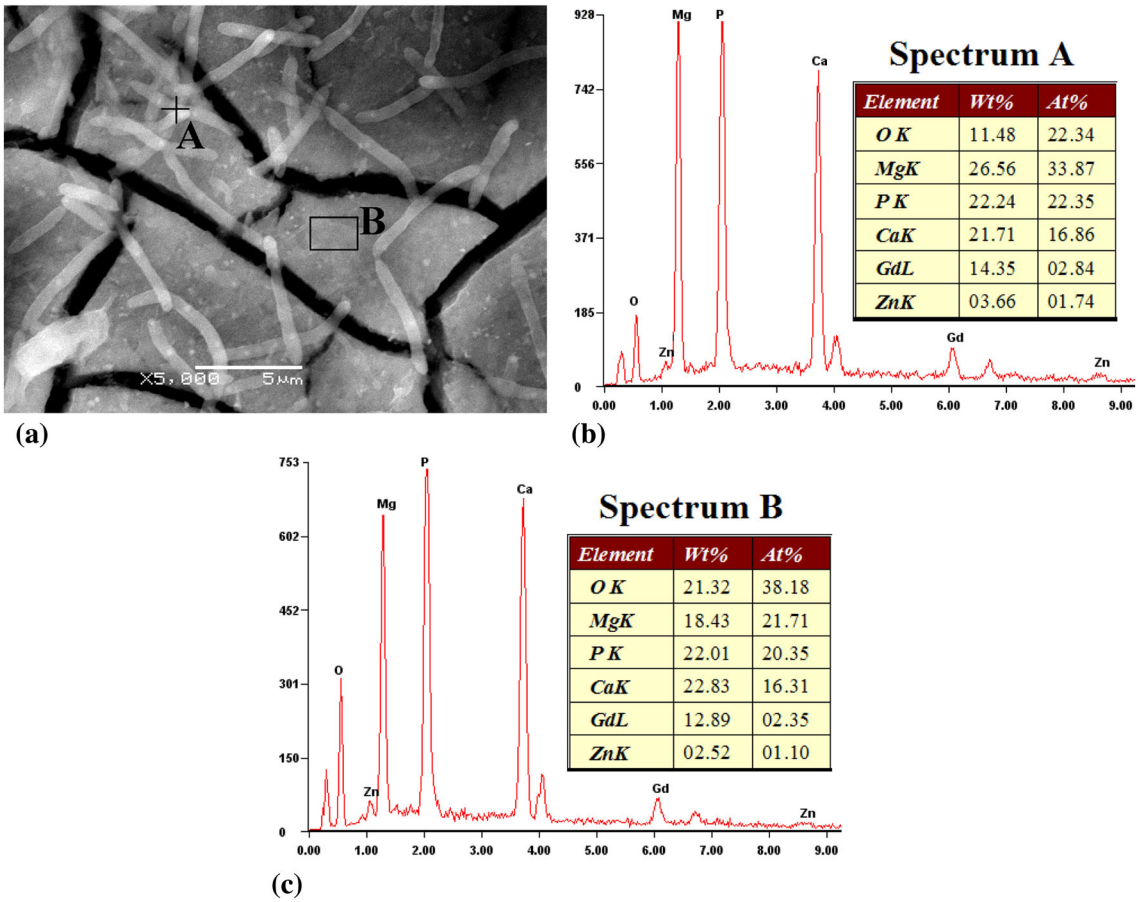

Fig. 5 Corrosion morphology of the EA200 (a) and EDS results (b, c)

The representative polarization curves of the alloys tested in SBF are shown in Fig. 8, and the results analyzed by Tafel extrapolation are listed in Table 1. The corrosion potential (E_{corr}) of the alloy after aging treatment is lower than the as-extruded alloy, revealing a negative corrosion resistance from the perspective of thermodynamics. The corrosion rates of the EA200 and EA220 calculated from the current density (i_{corr}) are higher and that of the EA180 is lower than that of the as-extruded one. The polarization results are not consistent with those obtained by mass loss test. It is mainly because the polarization test only shows instant corrosion rate of the alloy, while the mass loss test reflects a long-term corrosion rate of the alloy (Ref 28-30). According to the results in this work, the corrosion resistance of the alloy evaluated by mass loss is more reliable than that tested by polarization.

The LPSO structure plays a significant role in uniform corrosion mode according to the studies on the as-cast and solution-treated GZ51K alloys (Ref 9, 20). In the as-extruded and aged alloys, the microstructure is mainly composed of matrix grains with and without LPSO structure, and tiny precipitations. The precipitation is a corrosion-resistant phase and acts as cathode, which may cause galvanic corrosion. However, it did not impact the corrosion resistance significantly because of tiny and dispersive distribution. The GZ51K alloy immersed in SBF for 120 h shows uniform corrosion surface,

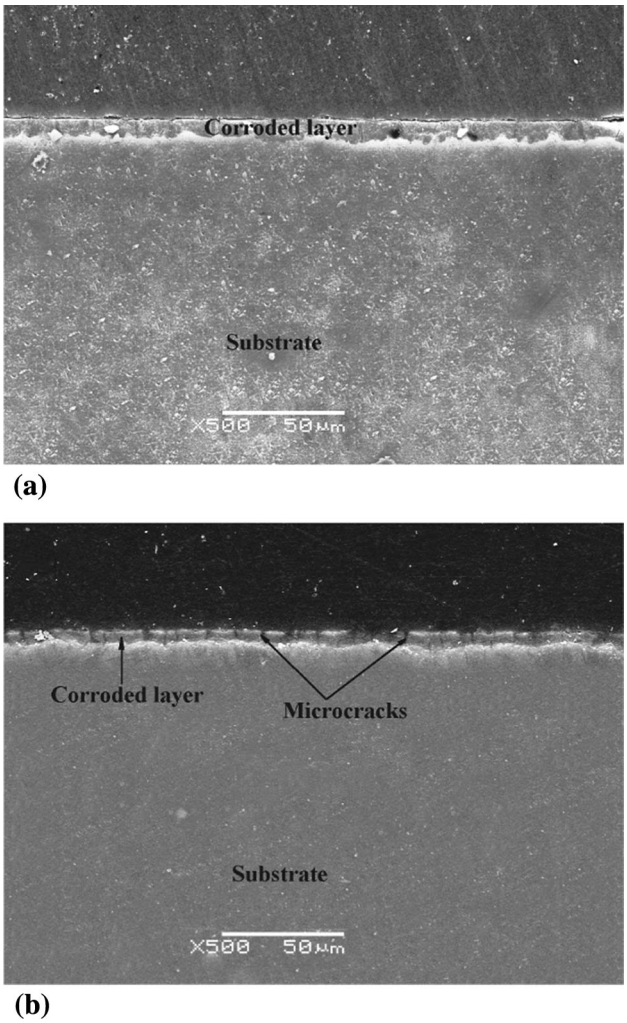

Fig. 6 Cross-section micrographs of the GZ51K alloys. (a) E and (b) EA200

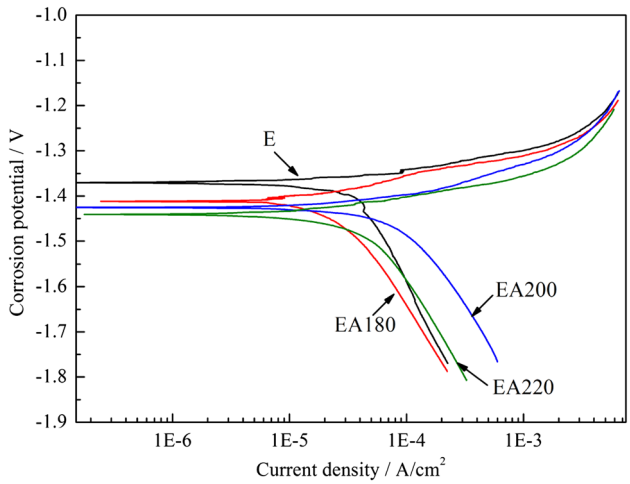

Fig. 8 Polarization curves of the GZ51K alloys

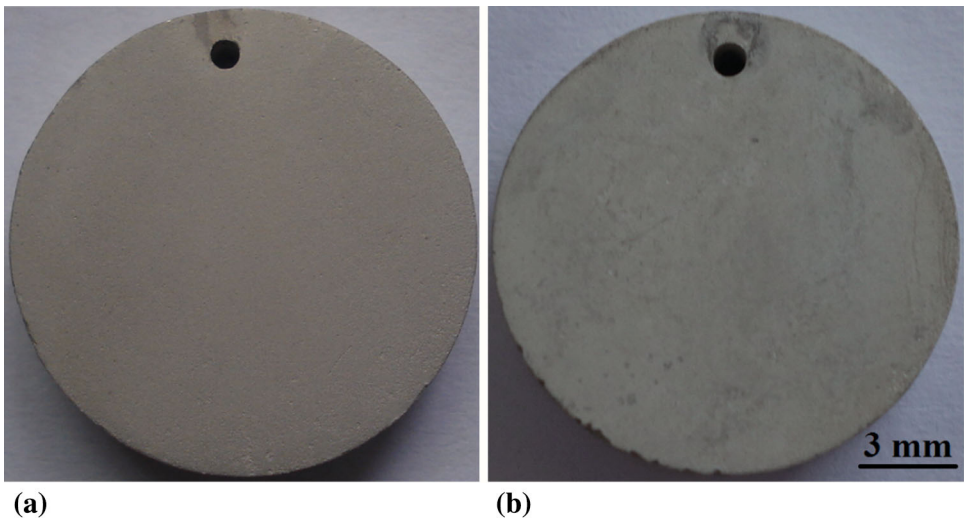

Fig. 7 Corroded surfaces of the GZ51K specimens after removing corrosion products. (a) E and (b) EA200

Table 1 Electrochemical parameters of the alloys obtained by Tafel extrapolation

Alloy	E_{corr}, V	i_{corr}, mA/cm^2	P_i, mm/year
E	−1.369	3.45×10^{-2}	0.79
EA180	−1.412	2.47×10^{-2}	0.56
EA200	−1.427	8.02×10^{-2}	1.83
EA220	−1.441	3.82×10^{-2}	0.87

while the commercial AZ91D immersed in SBF for 72 h presents severely localized corrosion (Ref 31). The unique microstructure of the GZ51K alloy with LPSO structure is responsible for the desirable uniform corrosion mode.

It has been reported that the corrosion resistance of the Mg-2Gd, Mg-5Gd, and Mg-10Gd binary alloys after aging treatment is improved apparently compared to the solution-treated alloys (Ref 32). Actually, on the one hand, the internal stress and crystal defects, such as vacuums and dislocations, are reduced due to the static recrystallization during aging treatment, and thus, improve corrosion resistance of the alloy. On the other hand, the tiny and uniformly distributed precipitation appears not to have had an adverse influence on corrosion resistance (Ref 32). Comprehensively, the enhanced corrosion resistance of the as-extruded alloy after aging treatment is likely attributed to the reduction of crystal defects and internal stress.

4. Conclusions

1. The microstructure of the as-extruded GZ51K alloy is composed of recrystallized α-Mg grains, long-elongated grains and precipitation, and most of the α-Mg grains have LPSO structure throughout whole grains. The long-elongated grains disappear after being aged at 200 and 220 °C because of the occurrence of static recrystallization.
2. The microhardness of the alloy after aging treatment is improved slightly, and the yield strength shows no visible enhancement. Nevertheless, the yield strength and elongation of both as-extruded and aged alloys are over 200 MPa and 25%, respectively, indicating a good combination of strength and ductility.
3. The corrosion rate of the as-extruded alloy is 0.92 mm/year, but it is reduced to 0.62, 0.50, and 0.53 mm/year after being aged at 180, 200, and 220 °C, respectively. The corrosion result evaluated by mass loss test is more reliable than that obtained by polarization test. Moreover, the GZ51K alloy with LPSO structure exhibits good uniform corrosion mode.

Acknowledgment

This project was supported by the National Natural Science Foundation of China (51301089), the Natural Science Foundation of Jiangsu Province (BK20130745), the Opening Project of Jiangsu Key Laboratory of Advanced Structural Materials and Application Technology (ASMA201503), and the Qing Lan Project of Jiangsu Province.

References

1. Y.F. Zheng, X.N. Gu, and F. Witte, Biodegradable Metals, *Mater. Sci. Eng. R*, 2014, **77**, p 1–34
2. Z.H. Wang, N. Li, R. Li, Y.W. Li, and L.Q. Ruan, Biodegradable Intestinal Stents: A Review, *Prog. Nat. Mater. Int.*, 2014, **24**, p 423–432
3. N.T. Kirkland, Magnesium Biomaterials: Past, Present and Future, *Corros. Eng. Sci. Technol.*, 2012, **47**, p 322–328
4. Y.J. Chen, Z.G. Xu, C. Smith, and J. Sankar, Recent Advances on the Development of Magnesium Alloys for Biodegradable Implants, *Acta Biomater.*, 2014, **10**, p 4561–4573
5. X. Li, C.L. Chu, L. Liu, X.K. Liu, J. Bai, C. Guo, F. Xue, P.H. Lin, and P.K. Chu, Biodegradable Poly-Lactic Acid Based-Composite Reinforced Unidirectionally with High-Strength Magnesium Alloy Wires, *Biomaterials*, 2015, **49**, p 135–144
6. H. Du, Z.J. Wei, X.W. Liu, and E.L. Zhang, Effects of Zn on the Microstructure, Mechanical Property and Bio-Corrosion Property of Mg-3Ca Alloys for Biomedical Application, *Mater. Chem. Phys.*, 2011, **125**, p 568–575
7. T. Li, H.L. Zhang, Y. He, N. Wen, and X.T. Wang, Microstructure, Mechanical Properties and In Vitro Degradation Behavior of a Novel Biodegradable Mg-1.5Zn-0.6Zr-0.2Sc Alloy, *J. Mater. Sci. Technol.*, 2015, **31**, p 744–750
8. H. Li, Q.M. Peng, X.J. Li, K. Li, Z.S. Han, and D.Q. Fang, Microstructures, Mechanical and Cytocompatibility of Degradable Mg-Zn Based Orthopedic Biomaterials, *Mater. Des.*, 2014, **58**, p 43–51
9. X.B. Zhang, Z.X. Ba, Q. Wang, Y.J. Wu, Z.Z. Wang, and Q. Wang, Uniform Corrosion Behavior of GZ51K Alloy with Long Period Stacking Ordered Structure for Biomedical Application, *Corros. Sci.*, 2014, **88**, p 1–5
10. H. Qin, Y.C. Zhao, Z.Q. An, M.Q. Cheng, Q. Wang, T. Cheng, Q.J. Wang, J.X. Wang, Y. Jiang, X.L. Zhang, and G.Y. Yuan, Enhanced Antibacterial Properties, Biocompatibility, and Corrosion Resistance of Degradable Mg-Nd-Zn-Zr Alloy, *Biomaterials*, 2015, **53**, p 211–220
11. C.Y. Zhao, F.S. Pan, S. Zhao, H.C. Pan, K. Song, and A.T. Tang, Preparation and Characterization of As-Extruded Mg-Sn Alloys for Orthopedic Applications, *Mater. Des.*, 2015, **70**, p 60–67
12. X.B. Zhang, G.Y. Yuan, X.X. Fang, Z.Z. Wang, and T. Zhang, Effects of Solution Treatment on Yield Ratio and Biocorrosion Behaviour of As-Extruded Mg-2.7Nd-0.2Zn-0.4Zr Alloy for Cardiovascular Stent Application, *Mater. Technol.*, 2013, **28**, p 155–158
13. X.B. Zhang, Y. Zhang, K. Chen, Z.X. Ba, Z.Z. Wang, and Q. Wang, Microstructure, Mechanical and Corrosion Properties of a Mg-Nd-Zn-Sr-Zr Alloys as Biodegradable Material, *Mater. Sci. Technol.*, 2015, **31**, p 866–873
14. K. Chen, J.W. Dai, and X.B. Zhang, Improvement of Corrosion Resistance of Magnesium Alloys for Biomedical Applications, *Corros. Rev.*, 2015, **33**, p 101–117
15. G. Manivasagam and S. Suwas, Biodegradable Mg and Mg Based Alloys for Biomedical Implants, *Mater. Sci. Technol.*, 2014, **30**, p 515–520
16. Y.S. Jeong and W.J. Kim, Enhancement of Mechanical Properties and Corrosion Resistance of Mg-Ca Alloys Through Microstructural Refinement by Indirect Extrusion, *Corros. Sci.*, 2014, **82**, p 392–403
17. L. Zhang, D. Zhang, Y. Dong, F. Guo, G. Hu, H. Xue, and F. Pan, Microstructure and Tensile Properties of As-Extruded and as Aged Mg-Al-Zn-Mn-Sn Alloy, *Mater. Sci. Technol.*, 2015, **31**, p 1088–1095
18. F. Liu, C.X. Chen, J.L. Niu, J. Pei, H. Zhang, H. Huang, and G.Y. Yuan, The Processing of Mg Alloy Micro-Tubes for Biodegradable Vascular Stents, *Mater. Sci. Eng. C*, 2015, **48**, p 400–407

19. X.B. Zhang, Y.J. Xue, Z.Z. Wang, X.C. He, and Q. Wang, Microstructure, Mechanical and Corrosion Properties of Mg-(4−x)Nd-xGd-Sr-Zn-Zr Biomagnesium Alloys, *Acta Metall. Sin.*, 2014, **50**, p 979–988
20. X.B. Zhang, Q. Wang, F.B. Chen, Y.J. Wu, Z.Z. Wang, and Q. Wang, Relation Between LPSO Structure and Biocorrosion Behavior of Biodegradable GZ51K Alloy, *Mater. Lett.*, 2015, **138**, p 212–215
21. X.B. Zhang, X.C. He, Y.J. Xue, Z.Z. Wang, and Q. Wang, Microstructure and Corrosion Resistance of as-cast Mg-Nd-Gd-Sr-Zn-Zr Alloys for Biomedical Applications, *Mater. Technol.*, 2014, **29**, p 179–187
22. J.S. Zhang, W.B. Zhang, L.P. Bian, W.L. Cheng, X.F. Niu, C.X. Xu, and S.J. Wu, Study of Mg-Gd-Zn-Zr Alloys with Long Period Stacking Ordered Structures, *Mater. Sci. Eng. A*, 2013, **585**, p 268–276
23. Y.J. Wu, L.M. Peng, X.Q. Zeng, D.L. Lin, W.J. Ding, and Y.H. Peng, A High Strength Extruded Mg-Gd-Zn-Zr Alloy with Superplasticity, *J. Mater. Res.*, 2009, **24**, p 3596–3602
24. K. Liu, J.H. Zhang, H.Y. Lu, D.X. Tang, L.L. Rokhlin, F.M. Elkin, and J. Meng, Effect of the Long Periodic Stacking Structure and W-phase on the Microstructures and Mechanical Properties of the Mg-8Gd-xZn-0.4Zr Alloys, *Mater. Des.*, 2010, **31**, p 210–219
25. F.M. Lu, A.B. Ma, J.H. Jiang, D.H. Yang, D. Song, Y.C. Yuan, and J. Chen, Effect of Multi-Pass Equal Channel Angular Pressing on Microstructure and Mechanical Properties of $Mg_{97.1}Zn_1Gd_{1.8}Zr_{0.1}$ Alloy, *Mater. Sci. Eng. A*, 2014, **594**, p 330–333
26. H.Y. Gao, K. Ikeda, T. Morikawa, K. Higashida, and H. Nakashima, Analysis of Kink Boundaries in Deformed Synchronized Long-Period Stacking Ordered Magnesium Alloys, *Mater. Lett.*, 2015, **146**, p 30–33
27. X.H. Shao, Z.Q. Yang, and X.L. Ma, Strengthening and Toughening Mechanisms in Mg-Zn-Y Alloy with a Long Period Stacking Ordered Structure, *Acta Mater.*, 2010, **58**, p 4760–4771
28. X.B. Zhang, Z.X. Ba, Z.Z. Wang, Y.J. Xue, and Q. Wang, Microstructure and Biocorrosion Behaviors of Solution Treated and As-Extruded Mg-2.2Nd-xSr-0.3Zr Alloys, *Trans. Nonferrous Met. Soc. China*, 2014, **24**, p 3797–3803
29. S. Manivannan, S.P.K. Babu, and S. Sundarrajan, Corrosion Behavior of Mg-6Al-1Zn-xRE Magnesium Alloy with Minor Addition of Yttrium, *J. Mater. Eng. Perform.*, 2015, **24**, p 1649–1655
30. N.T. Kirkland, N. Birbilis, and M.P. Staiger, Assessing the Corrosion of Biodegradable Magnesium Implants: A Critical Review of Current Methodologies and Their Limitations, *Acta Biomater.*, 2012, **8**, p 925–936
31. J.C. Zhou, Q. Li, H.X. Zhang, and F.N. Chen, Corrosion Behaviour of AZ91D Magnesium Alloy in Three Different Physiological Environments, *J. Mater. Eng. Perform.*, 2014, **23**, p 181–186
32. A. Atrens, M. Liu, and N.I.Z. Abidin, Corrosion Mechanism Applicable to Biodegradable Magnesium Implants, *Mater. Sci. Eng. B*, 2011, **176**, p 1609–1636